Nonlinear vibration mitigation of a crane's payload using pendulum absorber

Yurchenko, Daniil; Alevras, Panagiotis; Zhou, Shengxi; Wang, Junlei; Litak, Grzegorz; Gaidai, Oleg; Ye, Renchuan

DOI:
10.1016/j.ymssp.2020.107558

Passive vibration mitigation of a crane's payload

D. Yurchenko[1], P. Alevras[2], G. Litak[3], S. Zhou[4], O. Gaidai[5], R. Ye[6]

[1] IMPEE, Heriot-Watt University, Edinburgh, UK
[2] Mechanical Engineering Department, University of Birmingham, Birmingham, UK
[3] Faculty of Mechanical Engineering, Lublin University of Technology, Poland
[4]

[5]Jiangsu University of Science and Technology, Zhenjiang, China

Abstract

The paper proposes and investigates vibrations mitigation strategies of an externally harmonically excited pendulum. This problem is relevant to the crane's payload behavior, which dynamics is typically described by a lumped-mass pendulum model. Currently, there are various active control strategies to mitigate swinging vibrations of the payload, but there are no passive measures to achieve vibration mitigation. The proposed strategies involve the utilization of another pendulum which mass and length can be adjusted to hypothetically reduce the vibrations of the main system. Implementation of these strategies leads to the study of a double pendulum system. The paper presents results of the analytical study for the linearized model and numerical studies for the nonlinear model of the double pendulum system, describing their features.

Keywords

Tower cranes, Offshore cranes; Pendulum, Double pendulum, Pendulum tuned mass dampers, ~~Nonlinear energy sink,~~ Passive absorber, Vibrations mitigation

1 Introduction

Cranes remain an indispensable tool for heavy lifting in the construction sector as well as loading and unloading various cargos and goods from/to ships or lorries. Cranes are also actively used on ships and helicopters to conduct launch and recovery or rescue operations, which are the integral part of their daily routine. In fact, according to statistics about 35% of worldwide weather conditions have sea state 3 and higher, and in these conditions 50% of launch and recovery missions have to be suspended or aborted [1]. Moreover, in recent years many countries have been actively working on the development of unmanned boats and ships, where the onboard supervision of various routine processes and activities is simply impossible. Thus, these activities will have to be controlled and supervised remotely, which requires auxillary video monitoring systems, multiple sensors, data transmission units and other equipment to provide enough information about the ongoing and planned activities. Development of autonomous systems, including ROVs and UAVs has substantially increased the dependence on and role of cranes as well as their capabilities of performing routine operations remotely or completely autonomously. This is a highly challenging task, since nowadays all cranes operations are physically supervised by a crane operator, who heavily relies on his/her experience, knowledge and ability to adequately perceive the surrounding environment, including wind gusts, existing and/or suddenly

appearing static or moving obstacles, current position and velocity of the payload, etc. The situation aggravates substantially if the crane is positioned on a ship, operating in sea, where the roll, pitch and heavy motions of the ship are directly transmitted to the motion of the crane and crane's boom, exciting parametric vibrations [2],[3],[4]. It should be stressed that currently there are no systems that allow cranes to operate autonomously even in the perfectly calm sea.

Cranes can be classified by the degrees of freedom they have [5] and typically the payload motion is modelled as a lumped-mass system or mathematical pendulum. When the payload is moved by the crane or is excited by wind, it starts swinging oscillations, which may lead to various adverse effects, including cable breakdown or collision of the payload against other nearby objects. Controlling these oscillations is a difficult and may even seem as a counterintuitive task especially for an unexperienced operator. Indeed, the available control parameters, which can be adjusted, are the cable length and its reeling velocity, which both can influence the payload response parametrically by changing the cable length. Depending on the crane type various control strategies have been proposed and validated numerically and/or experimentally. Strategies based on H_∞ [6],[7], Neural Network [8],[9], nonlinear control [10],[11],[12], adaptive and input shaping control [13],[14],[15],[16],[17] optimal control [18],[19], vision control [20], sliding and saturated control [21],[22],[23],[24] PD control [25], hoisting control [26],[27] and combination of some of the above strategies [28],[29] were investigated and presented in the literature. The review papers [30],[31],[32], which comprehensively cover the existing literature up to 2017 and in the book [33] published in 2019 and references therein. It should be stressed that this topic, based on the number of publications in last three years, keeps attracting the attention of researchers all over the world due to the complex and nonlinear behavior of the payload, seeking for advanced and efficient mitigation strategies. Despite all these amazing control concepts, some effective control strategies are rather complex and assumes the existence of sensors that provides required information on the system state for decision making. In many practical applications the required sensors or sensor networks will be almost impossible to retrofit to the existing cranes. In some cases the processing and reaction time will be above the time required to make a decision. After all, any electronic system can fail leaving a crane operator to deal with the swinging payload. Thus, it seems reasonable to look for other possible options of mitigating swings of the payload, and one of such option can be a passive absorber.

Pendulum Tuned Mass Damper (PTMD) is a dynamic absorbing mechanism similar to a Tuned Mass Damper (TMD) [34],[35],[36], which can be used to absorb vibrations of an original system subjected to a harmonic or stochastic excitation. The tuning of a TMD is implemented by adding a secondary mass to the original oscillatory single-degree-of-freedom system, where the mass and the stiffness of the TMD are selected appropriately. In the case of a PTMD the tuning is not that obvious because, firstly the PTMD is inherently nonlinear since represents a pendulum, and secondly the natural frequency of the PTMD depends on its length, thus the original device should have enough space to accommodate the PTMD. The use of nonlinear isolators or energy sinks to mitigate adverse vibrations has been previously discussed [37],[38], however not in the context of the payload vibrations mitigation. The obvious advantage of such a passive device would be its ability to mitigate vibrations independently of a presented active control strategy and can improve the payload dynamics for remotely operating cranes.

Thus, the main motivation for this work is the aspiration of developing a passive vibration mitigation mechanism that can help conducting crane operations in safe and reliable manner. The basic idea behind the application of the PTMD for the payload vibration mitigation is shown in Figure 1, where the blue block is the original payload, and the orange block represents the PTMD. The original crane with the payload (Figure 1 left) of mass M, which represents the hook and the payload together, hanging at distance L from the suspension point. It is proposed to implement a

PTMD in two different ways:

1) Case I: the PTMD is suspended between the payload and the suspension point, so that $L=L_1+L_2$. In this case the payload has a hole where the main cable is going through and it can be controlled by an independent motor, thereby it can be retrofitted to an existing crane system. Moreover, the overall length of the cable is not increased, as can be seen in Figure 1 (middle), therefore this strategy can be very useful.
2) Case II: the PTMD is connected under the primary mass, so that $L=L_1$ and L_2 should be adjusted through the analysis. Since the PTMD is connected to the payload this approach can also be retrofitted to the existing crane systems, however, the overall length of the system will increase, creating problems with its handling and landing. Moreover, the overall mass of the payload will increase adding the PTMD mass and it will not be engaged at the beginning of lifting up when the secondary mass will be resting on the floor or floating on water.

Comment [PA(E1]: This part is slightly off-tune

The reader gets the impression that Case I is the one which will be shown to be better.

Obviously in both the cases implementing a PTMD creates a double-pendulum or two-degree-of-freedom system, which has naturally nonlinear behaviour. Thus, the adjustment or tuning of the parameters of the PTMD requires understanding the nonlinear dynamics of a double-pendulum system for adjusting the parameters of the PTMD in each case. It should be stressed that the typical goal of a TMD is to reduce the vibrations of the main mass, whereas the goal of a PTMD in the current application is to reduce the vibrations of both the systems, because large response of either mass can cause significant problems to a crane operator and the surrounding structures.

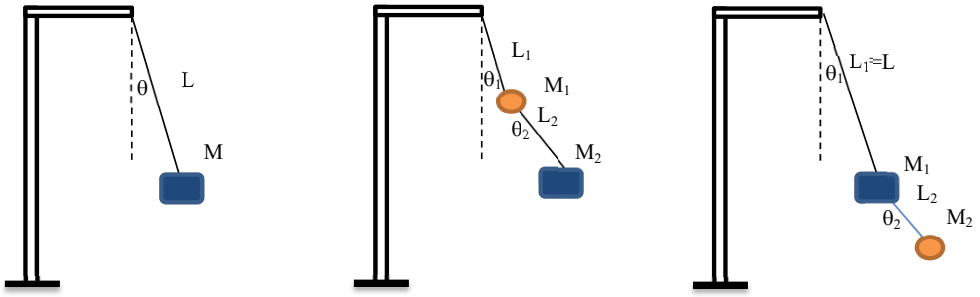

Figure 1. The original system (left), Case I (middle) and Case II (right).

Double-pendulum system has been intensively investigated by a number of authors in last several decades, including the presence of a chaotic response in some cases, which were experimentally observed and reported [39],[40]. Later, it has been shown [41],[42],[43] that a double pendulum is a non-integrable system that has a transversal homoclinic trajectory for any non-zero values of the parameters. Two integrable limiting cases were studied for the case of zero gravity and the case when the pendulums are uncoupled using Melnikov's approach [44], [45]. Influence of the double-pendulum variable mass, mass exchange and initial velocity were investigated in [46],[47],[48]. The behaviour of a parametrically excited double pendulum was studied in [49], whereas the energy harvesting using a double pendulum was reported in [50]. Despite all these advanced studies, none of the above works has explicitly studied a pendulum vibrations mitigation strategy using another pendulum i.e. PTMD. This paper proposes to study the effect of a pendulum absorber on other pendulum vibrations, including the characteristics features of classical linear and nonlinear responses and the influence of the given parameters on vibrations mitigation.

In this paper, the proposed passive absorbing methodology is studied analytically in the case of small vibrations, and numerically in the nonlinear case. In Section 2 the governing equations of

motion for a double pendulum system are derived using Newtonian approach. Section 3 studies Case I, where the PTMD is introduced between the payload and the suspension point. Section 4 studies Case II, where the PTMD is introduced below the payload, which resembles the case of a classical TMD. In Section 5 the approach similar to one developed in Section 4 is presented using a tri-pendulum system. The conclusions are presented in the last section of the paper.

2 External excitation of a payload

In this study it is assumed that the vibrations of the payload occurs due to a harmonic external force, applied to it, therefore one has to derive the equations of motion of the proposed TDOF system for both the cases. Thus, two forces F_1 and F_2 are introduced in Figure 2, which depicts the free body diagram of the model. Assume that $\theta_1$and θ_2 are the inclination angles of M_1 and M_2 correspondingly.

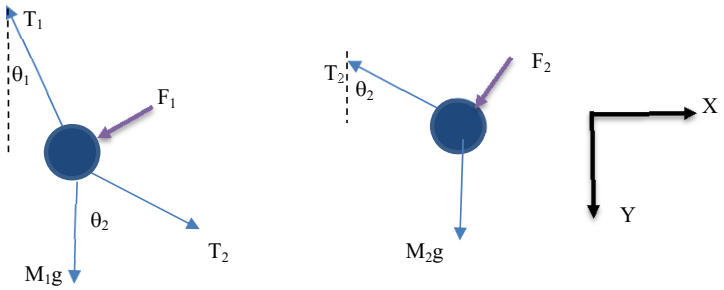

Figure 2. Free body diagram of the two-mass pendulum system

Following the notation and coordinated in Figure 2, the equations of motion for the first mass can be written as following:

$$\begin{cases} M_1L_1(\ddot{\theta}_1 cos\theta_1 - \dot{\theta}_1^2 sin\theta_1) = -T_1 sin\theta_1 + T_2 sin\theta_2 - F_1 cos\theta_1 \\ -M_1L_1(\ddot{\theta}_1 sin\theta_1 + \dot{\theta}_1^2 cos\theta_1) = -T_1 cos\theta_1 + T_2 cos\theta_2 + F_1 sin\theta_1 + M_1 g \end{cases} \quad (1)$$

Thus, simplifying this expression by multiplying the corresponding equations by sine and cosine functions, the first and second derivatives of the first angle can be expressed as:

$$\begin{cases} L_1\ddot{\theta}_1 = \frac{T_2}{M_1} sin(\theta_2 - \theta_1) - g sin\theta_1 - \frac{F_1}{M_1} \\ L_1\dot{\theta}_1^2 = \frac{T_1}{M_1} - \frac{T_2}{M_1} cos(\theta_2 - \theta_1) - g cos\theta_1 \end{cases} \quad (2)$$

Now, let's consider the second mass:

$$\begin{cases} M_2(L_1\ddot{\theta}_1 cos\theta_1 - L_1\dot{\theta}_1^2 sin\theta_1 + L_2\ddot{\theta}_2 cos\theta_2 - L_2\dot{\theta}_2^2 sin\theta_2) = -T_2 sin\theta_2 - F_2 cos\theta_2 \\ -M_2(L_1\ddot{\theta}_1 sin\theta_1 + L_1\dot{\theta}_1^2 cos\theta_1 + L_2\ddot{\theta}_2 sin\theta_2 + L_2\dot{\theta}_2^2 cos\theta_2) = -T_2 cos\theta_2 + F_2 sin\theta_2 + M_2 g \end{cases} \quad (3)$$

These equations can be used to derive the expression for the first and second derivative of the second angle in terms of the forces, suing the expressions (2):

$$\begin{cases} L_2\ddot{\theta}_2 = -\frac{T_1}{M_1}sin(\theta_2-\theta_1) + \frac{F_1}{M_1}cos(\theta_2-\theta_1) - \frac{F_2}{M_2} \\ L_2\dot{\theta}_2^2 = \frac{T_2}{M_2} + \frac{T_2}{M_1} - \frac{T_1}{M_1}cos(\theta_2-\theta_1) - \frac{F_1}{M_1}sin(\theta_2-\theta_1) \end{cases} \quad (4)$$

Using the first equations in (2) and (4) one can express the tensions T_1 and T_2:

$$\begin{cases} T_2 = \frac{M_1L_1\ddot{\theta}_1 + M_1gsin\theta_1 + F_1}{sin(\theta_2-\theta_1)} \\ T_1 = \frac{F_1cos(\theta_2-\theta_1) - \frac{M_1F_2}{M_2} - M_1L_2\ddot{\theta}_2}{sin(\theta_2-\theta_1)} \end{cases} \quad (5)$$

and substitute them into the second equations of (2) and (4) to arrive to the following equations of motion:

$$\begin{cases} L_1\dot{\theta}_1^2 = \frac{F_1cos(\theta_2-\theta_1)/M_1 - \frac{F_2}{M_2} - L_2\ddot{\theta}_2}{sin(\theta_2-\theta_1)} - \frac{L_1\ddot{\theta}_1 + gsin\theta_1 + F_1/M_1}{sin(\theta_2-\theta_1)}cos(\theta_2-\theta_1) - gcos\theta_1 \\ L_2\dot{\theta}_2^2 = \frac{M_1L_1\ddot{\theta}_1 + M_1gsin\theta_1 + F_1}{M_2sin(\theta_2-\theta_1)} + \frac{L_1\ddot{\theta}_1 + gsin\theta_1 + \frac{F_1}{M_1}}{sin(\theta_2-\theta_1)} - \\ -\frac{F_1cos(\theta_2-\theta_1)/M_1 - \frac{F_2}{M_2} - L_2\ddot{\theta}_2}{sin(\theta_2-\theta_1)}cos(\theta_2-\theta_1) - \frac{F_1}{M_1}sin(\theta_2-\theta_1) \end{cases} \quad (6)$$

which can be simplified:

$$\begin{cases} L_2\ddot{\theta}_2 + L_1\ddot{\theta}_1cos(\theta_2-\theta_1) = -\frac{F_2}{M_2} - L_1\dot{\theta}_1^2sin(\theta_2-\theta_1) - gsin\theta_2 \\ \left(\frac{M_1}{M_2}+1\right)L_1\ddot{\theta}_1 + L_2\ddot{\theta}_2cos(\theta_2-\theta_1) = -\frac{F_2}{M_2}cos(\theta_2-\theta_1) - \\ -\frac{F_1}{M_2} - \left(\frac{M_1}{M_2}+1\right)gsin\theta_1 + L_2\dot{\theta}_2^2sin(\theta_2-\theta_1) \end{cases} \quad (7)$$

The first and second equations can be simplified by introducing $\mu = \frac{M_2}{M_1+M_2}, \eta = L_1/L_2$ and dividing both sides of the equations correspondingly:

$$\begin{cases} \ddot{\theta}_2 + \eta\ddot{\theta}_1cos(\theta_2-\theta_1) = -\frac{F_2}{M_2L_2} - \eta\dot{\theta}_1^2sin(\theta_2-\theta_1) - \Omega_2^2sin\theta_2 \\ \eta\ddot{\theta}_1 + \mu\ddot{\theta}_2cos(\theta_2-\theta_1) = -\mu\frac{F_2}{M_2L_2}cos(\theta_2-\theta_1) - \frac{\mu}{L_2}\frac{F_1}{M_2} - \Omega_2^2sin\theta_1 + \mu\dot{\theta}_2^2sin(\theta_2-\theta_1) \end{cases} \quad (8)$$

where $\Omega_2^2 = g/L_2$. This set of nonlinear ODEs should be solved in order to predict behaviour of the payload and to adjust the secondary mass's parameters and it will be done for each case separately. Classical Lagrange approach can be used to derive the system's governing equations of motion and it is presented in Appendix.

3 Case I: the PTMD is above the payload and F_1=0

In this case the PTMD mass M_1 is on top of the payload mass M_2, and since it is relatively small, the force F_1 acting on it will be neglected. Moreover, since $L = L_1 + L_2$, and $L_1 = \eta L_2$, then $L = L_2(1+\eta)$ and

$$\Omega_2^2 = \frac{g}{L_2} = \frac{g}{L}\frac{L}{L_2} = \Omega^2(1+\eta) \quad (9)$$

where $\Omega^2 = g/L$ is the natural frequency of the original system, i.e. the payload. Taking into account the above arguments, adding a linear damping term to the first equation representing friction between the cable in the suspension point, one can rewrite the equations of motion as:

$$\begin{cases} \ddot{\theta}_2 + \eta\ddot{\theta}_1 cos(\theta_2 - \theta_1) = -c\dot{\theta}_1 \ - \frac{F_2}{M_2 L_2} - \eta\dot{\theta}_1^2 sin(\theta_2 - \theta_1) - \Omega^2(1+\eta)sin\theta_2 \\ \eta\ddot{\theta}_1 + \mu\ddot{\theta}_2 cos(\theta_2 - \theta_1) = -\mu\frac{F_2}{M_2 L_2} cos(\theta_2 - \theta_1) - \Omega^2(1+\eta)sin\theta_1 + \mu\dot{\theta}_2^2 sin(\theta_2 - \theta_1) \end{cases} \quad (10)$$

3.1 Linearized dynamics

To study small oscillations one can use the linearized equations (10) assuming $sin\theta_i = \theta_i$, $\cos[\theta_2 - \theta_1] = 1$, i=1,2) and rewrite the equations as following:

$$\begin{gathered} \eta\ddot{\theta}_1 + \mu\ddot{\theta}_2 + \Omega^2(1+\eta)\theta_1 + c\dot{\theta}_1 \ = -f_0\mu \\ \ddot{\theta}_2 + \eta\ddot{\theta}_1 + \Omega^2(1+\eta)\theta_2 = -f_0, \ where \ f_0 = \frac{F_2}{M_2 L_2} = \frac{F_2}{M_2 L}(1+\eta) \end{gathered} \quad (11)$$

When the excitation is a harmonic process and $F_2(t) = \lambda M_2 L \exp(i\omega t)$, so that $f_0 = \lambda \exp(i\omega t)(1+\eta)$, then the solution can be sought in the same form, namely $\theta_1(t) = A_1 \exp(i\omega t)$ and $\theta_2 = B_1 \exp(i\omega t)$, which after substitution yields:

$$\begin{gathered} [-\omega^2\eta + \Omega^2(1+\eta) + ic\omega]\mathrm{A}_1 + [-\omega^2\mu]\mathrm{B}_1 = -\mu\lambda(1+\eta) \\ -\omega^2\eta\mathrm{A}_1 + [-\omega^2 + \Omega^2(1+\eta)]\mathrm{B}_1 = -\lambda(1+\eta) \end{gathered} \quad (12)$$

It is relatively straightforward to find a solution of these two equations:

$$\begin{aligned} \mathrm{A}_1 &= -\frac{\lambda\mu\Omega^2(1+\eta)^2}{\left[\omega^4\,\eta(1-\mu) + (1+\eta)^2\Omega^2(\Omega^2 - \omega^2)\right]} \\ \mathrm{B}_1 &= -\frac{\lambda(1+\eta)\left[\left(\Omega^2(1+\eta) - \eta(1-\mu)\omega^2\right)\right]}{\left[\omega^4\,\eta(1-\mu) + (1+\eta)^2\Omega^2(\Omega^2 - \omega^2)\right]} \end{aligned} \quad (13)$$

The second equation can be further rearranged in the following way for the undamped case:

$$\left|\frac{\mathrm{B}_1\Omega^2}{\lambda}\right| = \left|\frac{(1+\eta)(1+\eta-\eta(1-\mu)\mathrm{n}^2)}{\mathrm{n}^4\,\eta(1-\mu)+(1+\eta)^2(1-\mathrm{n}^2)}\right|, \mathrm{n} = \frac{\omega}{\Omega} \quad (14)$$

Obviously, in the resonant case (n=1) the expression in the numerator is not equal to zero, which indicates that the use of PTMD in this arrangement does not lead to the desired result, i.e. does not reduce the vibrations of the payload to zero. In fact, in this case, the non-dimensional amplitude of the payload will be inversely proportional to $(1-\mu)$, making it relatively high for relatively small values of the PTMD mass:

$$\left|\frac{\mathrm{B}_1\Omega^2}{\lambda}\right| = \left|\frac{(1+\eta\mu)(1+\eta)}{\eta(1-\mu)}\right| \quad (15)$$

Although this value remains finite for any nonzero value of the PTMD mass, the response may still be high. In other cases of near the resonance values of n, the proposed methodology provides reduction of the response amplitude compared to the response of the original system. It is well

known that the undamped response of the original payload is inversely proportional to $|\Omega^2 - \omega^2|$ and will have high but finite response amplitude within the system bandwidth except the resonance frequency. The contour plots presented in Figure 3 are produced from (14) for different values of n. Each sub-figure has been plotted for different values of the frequency ratio n and presents a map in the μ, η -space. One can observe from Figure 3 that the structure of the plot changes after crossing the resonance value n=1, although the overall advantageous effect of increasing η can be observed throughout all the plots. For the values of the excitation frequency below the resonance n<1, shown in Figures 3a-3b the maps have very similar pattern of steeply increasing curves with their values increasing to the right. One can also deduce that to increase the effect of PTMD its mass should be increased, whereas for a given PTMD mass value the value of η should be increased. However, the far from resonance response (n<1) as in Figure 3a, one can also see that the response does not depends much, when values of $\eta > 1$, because the curves reduces to almost vertical lines. For closer to the resonance values of n (Figure 3b) the curves bend to the left more and more providing an optimal pair of η, μ values corresponding to a minimal response amplitude. Passing the resonance makes the curves bend to the left more and the response values will now decrease with the increase of μ.

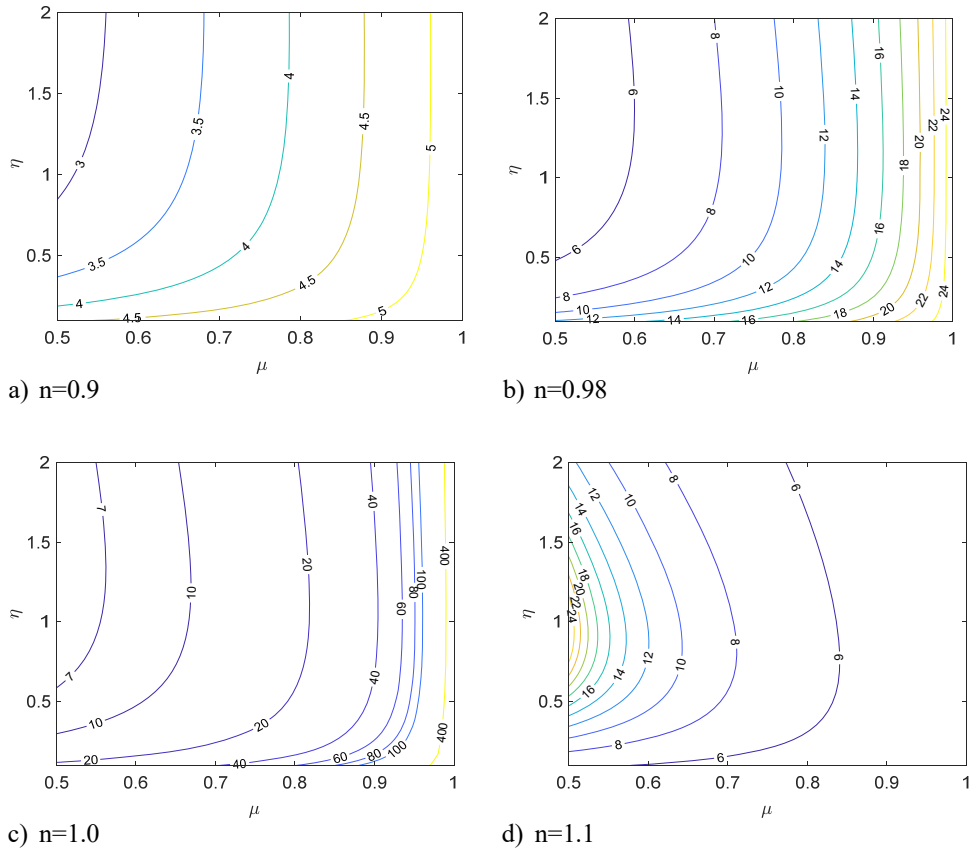

a) n=0.9 b) n=0.98

c) n=1.0 d) n=1.1

Figure 3. Contour maps of non-dimensional amplitude (14) for $\Omega^2 = 1$, and varying μ, η and n.

Passing the resonance, the structure of the contour lines changes drastically, and now it is possible to select values of η and μ such that the response of the payload with the PTMD becomes worse than that without PTMD. This effect has not been observed in the pre-resonance domain, where any set of parameters η and μ result in a mitigated response, and is due to the

second peak, introduced by implementing the PTMD.

3.2 Numerical analysis of the nonlinear absorber

To study the effect of the nonlinearity onto the system performance the full set of equations will be modelled numerically:

$$\ddot{\theta}_2 + \eta\ddot{\theta}_1 cos(\theta_2 - \theta_1) = -\frac{F_2(1+\eta)}{M_2 L} - \eta\dot{\theta}_1^2 sin(\theta_2 - \theta_1) - \Omega_2^2 sin\theta_2$$
$$\eta\ddot{\theta}_1 + \mu\ddot{\theta}_2 cos(\theta_2 - \theta_1) = -\mu\frac{F_2(1+\eta)}{M_2 L} cos(\theta_2 - \theta_1) - \Omega_2^2 sin\theta_1 + \mu\dot{\theta}_2^2 sin(\theta_2 - \theta_1) \quad (16)$$

$$F_2(t) = \lambda M_2 L \sin(\omega t)$$

The above equations of motion are analyzed through numerical quasi-static continuation in the excitation frequency ω. The examined frequency range is selected to cover realistically low frequencies, centered around the resonance frequency of the primary system. The latter is assumed to correspond to a hanging payload at L=20m. The tracked quantity is the horizontal displacement amplitude of the payload, given by $x_p = L_1 \sin\theta_1 + L_2 \sin\theta_2$.

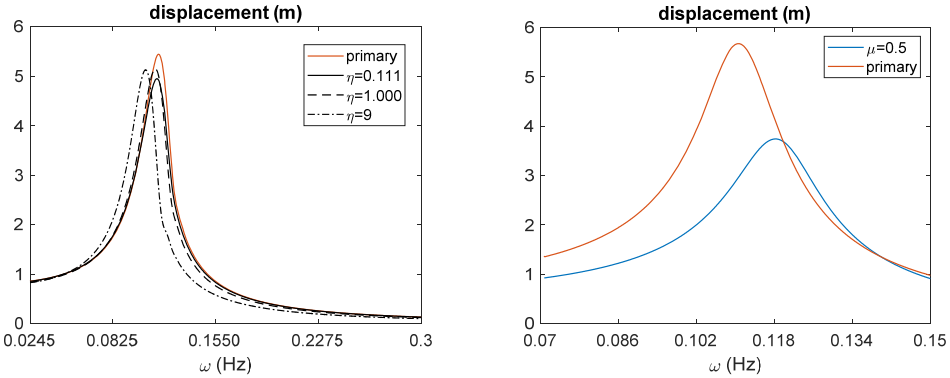

Figure 4. Frequency response curves for Case I

The numerical results of the payload amplitude shown in Figure 4 reveal that the configuration considered in Case I has very limited capacity to suppress the payload vibrations, even if the absorber attains unrealistically high weight. This is expected from the linearized analysis, and it is due to the fact that the mode shape introduced to the system with the addition of the absorber is confined to relatively high frequencies. Figure 4 left demonstrates the response amplitude-frequency curves of the primary mass x_p without absorber and with absorber at different lengths with respect to the payload length generated by the nonlinear set of equations (16) for μ=0.95. One can see a minor shift in the resonance frequency for the system with the absorber, and very insignificant decrease in the response amplitude even for large values of the length ratio η. Figure 4 right presents the payload response with the absorber as heavy as the mass of the payload for η=1. In this case a significant frequency shift and an amplitude reduction can be seen. Figures 5a and 5b demonstrate the contour plots of the absorber and payload correspondingly in the η–μ plane for the resonant case of n=1. One can see high values of the amplitude of the absorber

Comment [PA(E2]: Do you mean Figure 4 or Figure 5?

and payload are concentrated at high values of μ, which corresponds to a low value of the absorber mass. Moreover, the payload amplitude is high for any value of the mass ratio and low values of η.

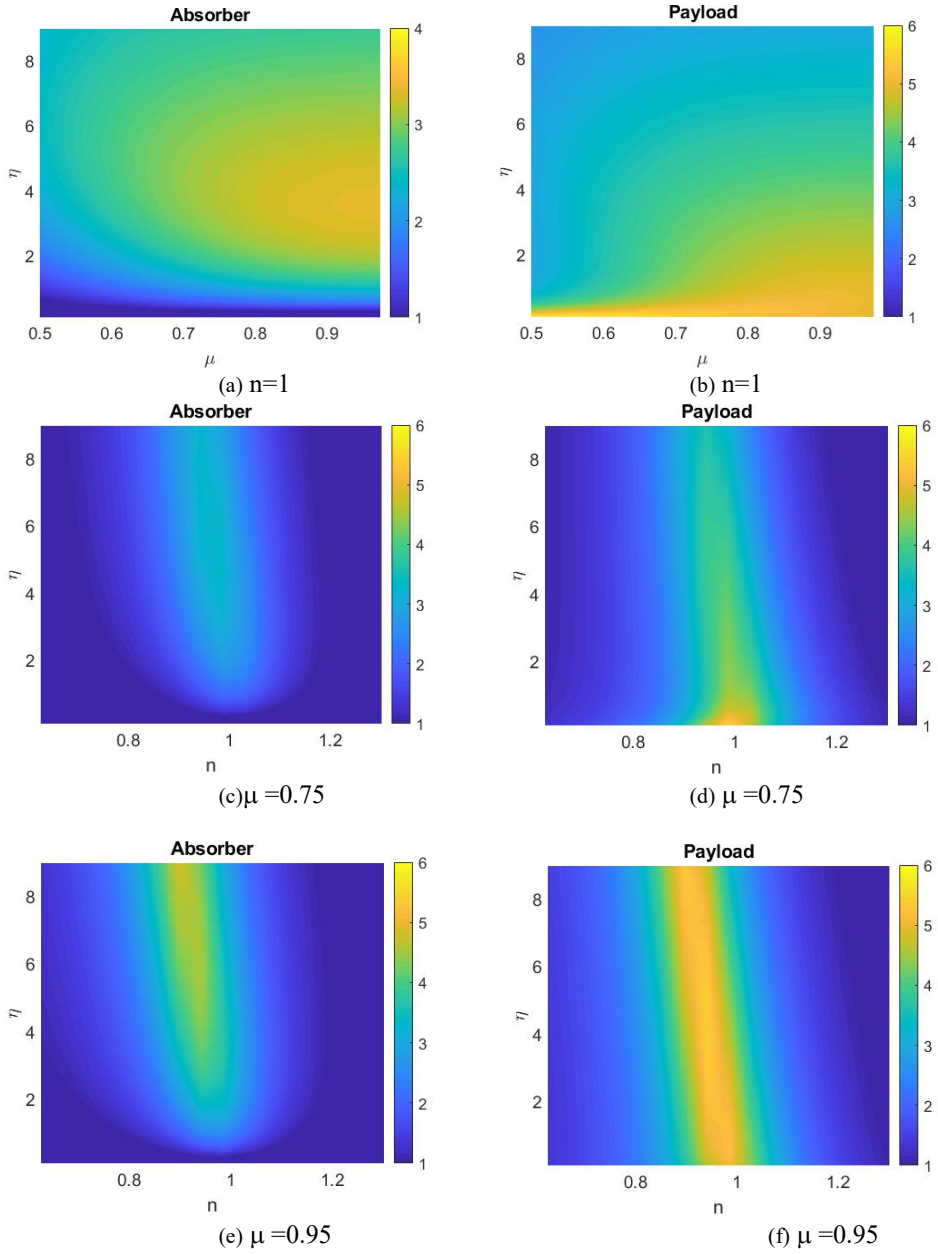

(a) n=1 (b) n=1

(c)μ =0.75 (d) μ =0.75

(e) μ =0.95 (f) μ =0.95

Figure 5. Contour plots for Case I and: the resonant case (a) and (b); value of μ =0.75 (c) and (d); value of μ =0.95 (e) and (f);

Relative effective energy absorption can be seen at high values of μ and η around 3.5, corresponding to large yellow region. However, since a high oscillation amplitude of the payload may also cause a collision against the ship hull, high swinging amplitudes of the payload and

absorber should be avoided. Thus, significant reduction of the amplitude of both the systems can be seen only for high absorber mass (low μ values). Figure 5 c – 5f demonstrate the contour maps η-n for values of μ =0.75 (middle raw) and μ=0.95 (bottom raw) correspondingly. The trail of yellow in the payload maps, especially bright at the bottom raw, demonstrates the poor performance of the absorber at the resonance, although its tilt to the left indicates the frequency shift without any amplitude reduction. In general one can conclude that the proposed strategy can be effective only for high values of the absorber mass, otherwise it will not be capable of mitigating the vibrations by absorbing the payload energy.

4 Case II: The PTMD is below the payload and F_2=0

In the second case the secondary mass M_2 is connected to the payload, so that the payload becomes M_1. Moreover, L=L_1 and L_2 can be any, thus $\Omega_2^2 = \Omega^2\,\eta$ according to its definition. Then, the force acting onto the secondary mass is neglected, i.e. F_2=0, so that the full set of equations is:

$$\begin{cases} \ddot{\theta}_2 + \eta\ddot{\theta}_1 cos(\theta_2 - \theta_1) = -\eta\dot{\theta}_1^2 sin(\theta_2 - \theta_1) - \Omega_2^2 sin\theta_2 \\ \eta\ddot{\theta}_1 + \mu\ddot{\theta}_2 cos(\theta_2 - \theta_1) = -\dfrac{\mu}{L_2}\dfrac{F_1}{M_2} - \Omega_2^2 sin\theta_1 + \mu\dot{\theta}_2^2 sin(\theta_2 - \theta_1) \end{cases}$$

where $\mu \ll 1$ now will have to be selected close to zero in order to make the secondary mass small, since M_2<< M_1 following the main idea of the TMD theory and according to the definition of μ above.

4.1 Investigation of the linear behavior

In the case of the small oscillations the above equations will be simplified as:

$$\ddot{\theta}_2 + \eta\ddot{\theta}_1 = -\Omega^2\,\eta\theta_2$$
$$\eta\ddot{\theta}_1 + \mu\ddot{\theta}_2 = -\frac{\mu\eta}{L}\frac{F_1}{M_2} - \Omega^2\,\eta\theta_1$$

Therefore, assuming $F_1(t) = \lambda M_2 L \exp(i\omega t)$, one can write the solution in the form of $\theta_1(t) = C_1 \exp(i\omega t)$ and $\theta_2 = D_1 \exp(i\omega t)$, which after substitution results in two algebraic equations:

$$[-\omega^2\eta]C_1 + [-\omega^2 + \Omega^2\eta]D_1 = 0$$
$$-\omega^2\mu D_1 + [-\omega^2\eta + \Omega^2\eta]C_1 = -\lambda\mu\eta$$

Solution of these equations can be written as:

$$C_1 = -\frac{\lambda\mu[\Omega^2\eta - \omega^2\,]}{(\Omega^2\eta - \omega^2\,)(\Omega^2 - \omega^2\,) - \mu\omega^4}$$
$$D_1 = -\frac{\lambda\eta\mu\omega^2}{(\Omega^2\eta - \omega^2\,)(\Omega^2 - \omega^2\,) - \mu\omega^4} \qquad (17)$$

It can be seen directly from the above expression that the payload amplitude can reach zero when the cable length of the secondary mass is equal to that of the payload, e.g. $\eta = 1$. This makes almost impossible, at least within the linear framework, to effectively mitigate payload vibrations since the required length cannot be achieved immediately after the begging of the lifting up process.

4.2 Nonlinear dynamics of the system

Here, a numerical study of the original nonlinear system will be conducted, with the external harmonic excitation in the form $F_1(t) = \lambda M_2 L \sin(\omega t)$ and additional damping terms:

$$\ddot{\theta}_2 + \eta\ddot{\theta}_1 cos(\theta_2 - \theta_1) = -\eta\dot{\theta}_1^2 sin(\theta_2 - \theta_1) - \Omega^2\, \eta sin\theta_2 + d_1\theta_1'$$
$$\eta\ddot{\theta}_1 + \mu\ddot{\theta}_2 cos(\theta_2 - \theta_1) = -\frac{\mu\eta}{L}\frac{F_1}{M_2} - \Omega^2\, \eta sin\theta_1 + \mu\dot{\theta}_2^2 sin(\theta_2 - \theta_1) + d_2\theta_2' \qquad (18)$$

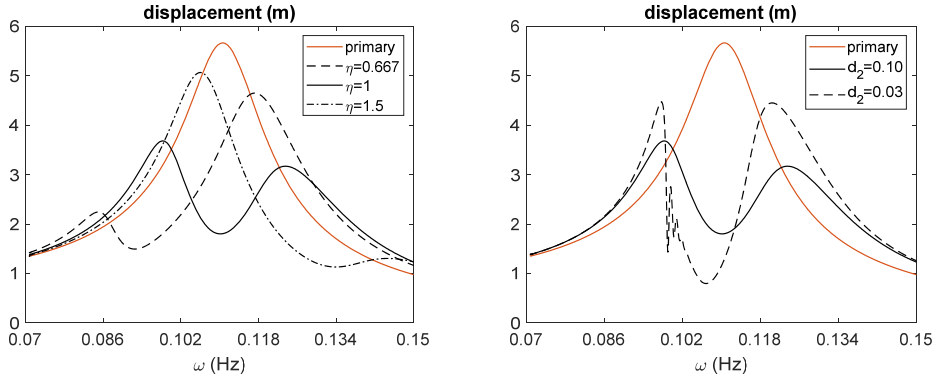

Figure 6. Frequency response curves for Case II

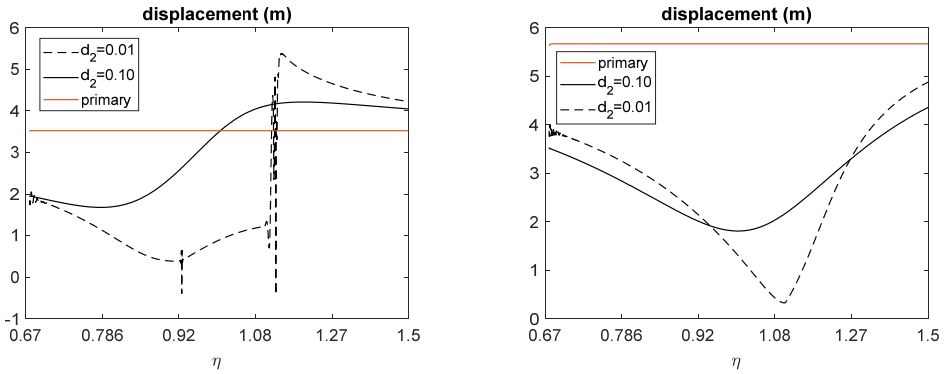

a) b)

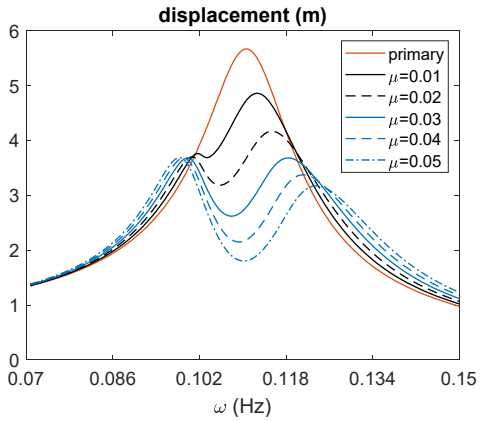

c)

Figure 7. Parametric analysis with respect to $\boldsymbol{\eta}$ and $\boldsymbol{\mu}$ for $\boldsymbol{d_2 = 0.1}$.

Figures 6 left presents the amplitude-frequency curves of the payload without any absorber (primary) and with the absorbers in the case of nonlinear oscillations, governed by Eq. (18) for μ=0.05 and d_2=0.1. One can observe that for η =1 the payload amplitude is reduced significantly

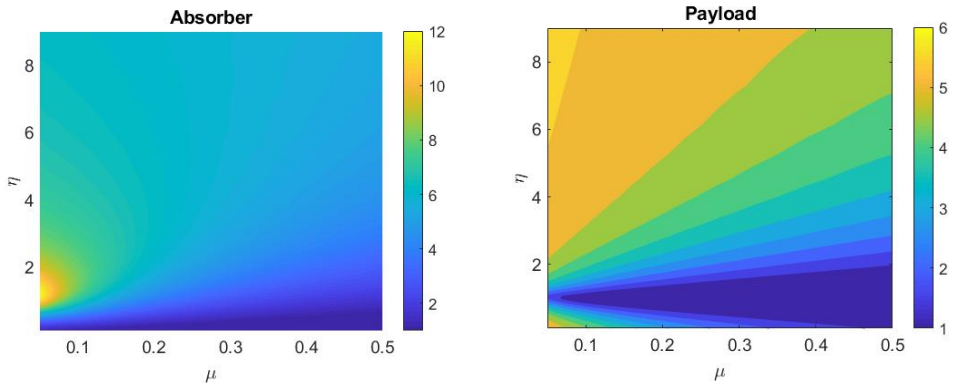

(a)n=1 (b) n=1

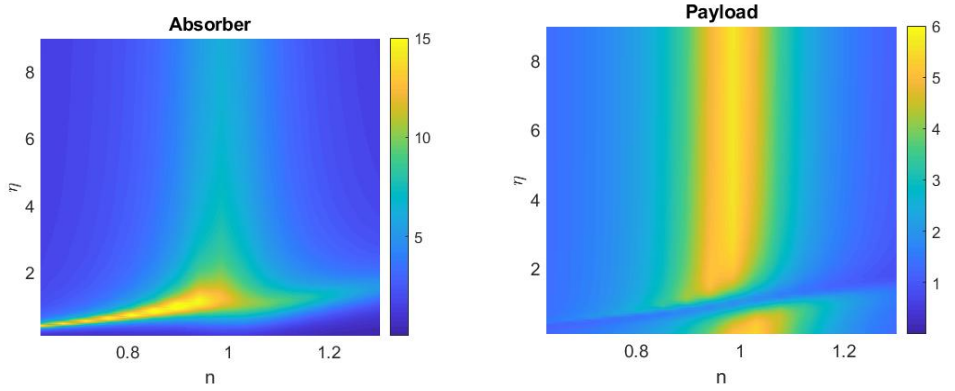

(c) μ =0.05 (d) μ =0.05

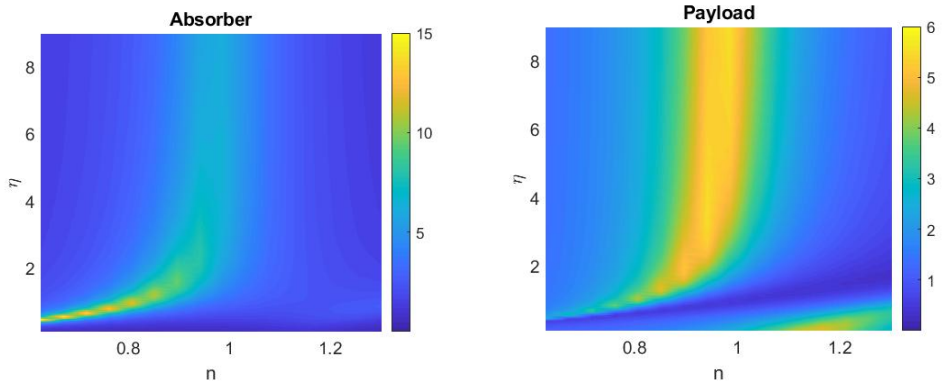

(e) μ =0.25 (f) μ =0.25

Figure 8. Parametric analysis with respect to $\boldsymbol{\eta}$ and $\boldsymbol{\mu}$ for: (a) n=1 (b) n=1 (c) $\boldsymbol{\mu}$ =0.05 (d) $\boldsymbol{\mu}$ =0.05 (e) $\boldsymbol{\mu}$ =0.25 (f) $\boldsymbol{\mu}$ =0.25

at the resonance. Figure 6 right for μ=0.05 and η =1 demonstrate the dependence of the payload response amplitude on the non-dimensional damping coefficient d_2. One can observe that the higher damping ratio can improve the response of the payload by reducing its amplitude. However, in this case it is hard to control the damping, since the absorber is connected to the payload by a hoist and other additional damping mechanics, will required additional design and efforts. Figure 7a and 7b present the payload response for μ=0.05 and values of $\Omega = 0.628$ and $\Omega = 0.691$ correspondingly. One can see that the high value of damping ratio leads to smoother response, however, the value of η is extremely important and the system response can be higher than that without the absorber if a wrong value of η is selected. In fact, the achieved mitigation at different frequencies can be reliant on the designed η values, as Figures 7a and 7b show. Note that these plots were produced with numerical forward sweep continuation, which gives rise to some transient responses around η=0.9 and η=1.1 in Figure 7a. However, such trajectories out of scope for the purpose of this paper. Figure 7c demonstrates the payload amplitude dependence on the mass ratio for the optimal linear value of η =1. A reasonable amplitude reduction over the entire range was observed for values of μ>0.03. Figure 8 presents a number of maps, which can be used for designing the optimal absorber. Figures 8a and 8b demonstrate the absorber and payload response in η–μ plane for n=1. A large blue strip corresponding to a low amplitude response can be found simultaneously at both the maps for the entire range of μ values and around η =1, which was expected. However, it should be stressed that this strip narrow down for low values of μ giving much less flexibility for the selection of η value. Moreover, the absorber map demonstrates the peak response amplitude at low values of μ and η value around 1.5. This also should be carefully considered since the absorber is supposed to be below the payload and its high amplitude vibrations may cause a collision. Next 4 plots, presented in Figures 8c-8f show the results in the η-n plane, where the clear amplitude reduction can be seen at the resonance (n=1) and η =1. It should be noted that the blue strip, looking like a straight line, can provide minimum response amplitude to the left and right from the resonance, pointing toward optimal values of the absorber for different frequency ratio. To conclude this part one should remember that although a great vibration mitigation can be achieved in this case, keeping the length ratio η =1 for all the hoisting time, it is simply impossible to keep this ratio at the begging of lifting. The reason is that at the begging of lifting the absorber should have the longest length while it is resting on the ground, thus practically staying useless up to a certain time instant, when the payload reaches its half uplifting distance. Thus, other options have to be investigated to develop a better absorber.

Comment [YD3]: Panos, explain here jumps!

5 Case III: Effective vibration mitigation strategy using tri-pendulum

It was shown above that neither Case I nor Case II can achieve satisfactory practical result for vibration mitigation. In some cases, especially when the launch and recovery operations have to be conducted in rough sea, a cage can be used to capture the floating object before lifting it up. These cages are large enough to accommodate an ROV, UAV or Tether Management Systems (TMSs) and sturdy to hold their weight. Taking into account this fact, next a case of a compound pendulum added to the payload cage is proposed. In particular, an N-pendulum [51] is considered as a potential candidate for the vibration mitigation of the payload since its natural frequency and length can be independently tuned. Moreover, apart from a classical compound pendulum, which shape defines the natural frequency, the proposed N-pendulum can be actively tuned to different excitation frequencies broadening its frequency range. Figure 9 demonstrates the proposed vibration mitigation system with tri-pendulum (N=3). The tri-pendulum consists of 3 separate arms situated at 120^o from each other and connected to a common hub placed on a bearing, such that the arms with a hub can oscillate around its suspension point. Each arm has a mass M_i placed at distance h_i from the hub. Keeping all three masses the same, the tri-pendulum can be tuned by adjusting the corresponding distances. The simplest case of $h_1>h_2=h_3$, as well as some other cases and the dependence of the N-pendulum natural frequency on the number of arms were studied in [51].

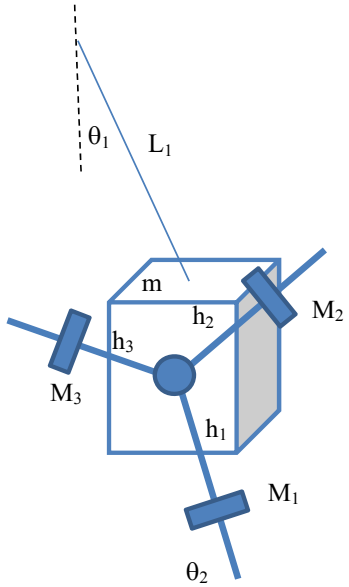

Figure 9. Tri-pendulum system

Using the Lagrange approach one can derive the governing equation of motion (see Appendix for derivations), assuming that $M_1= M_2= M_3=M$, $h_2= h_3$. Adding the damping and force terms into the equations they can be rewritten as:

$$\begin{gathered}(m+3M)l_1^2\theta_1'' + Ml_1(h_1-h_2)\,\theta_2''\cos(\theta_1-\theta_2) + Ml_1(h_1-h_2)\theta_2'^{\,2}\sin(\theta_1-\theta_2) \\ +(m+3M)g\,l_1\sin\theta_1 + c_1\theta_1' = -F_1l_1 \\ (h_1^2+2h_2^2)M\theta_2'' + Ml_1(h_1-h_2)\theta_1''\cos(\theta_1-\theta_2) + Ml_1(h_1-h_2)\theta_1'^{\,2}\sin(\theta_1-\theta_2) \\ +Mg(h_1-h_2)\sin\theta_2 + c_2\theta_2' = 0\end{gathered} \quad (19)$$

Introducing a set of non-dimensional parameters:

$$\mu = \frac{M}{m+3M}, \gamma = \frac{h_1}{h_2}, \eta = \frac{l_1}{h_2}, f_1 = \frac{F_1}{(m+3M)l_1}, d_1 = \frac{c_1}{(m+3M)l_1^2}, d_2 = \frac{c_2}{(m+3M)l_1^2} \quad (20)$$

one can rewrite:

$$\begin{aligned} \theta_1'' + \mu\frac{(\gamma-1)}{\eta}\theta_2'' \cos(\theta_1-\theta_2) + \mu\frac{(\gamma-1)}{\eta}\theta_2'^2 \sin(\theta_1-\theta_2) + \Omega_1^2 \sin\theta_1 + d_1\theta_1' = -f_1 \\ \theta_2'' + \frac{\eta(\gamma-1)}{(\gamma^2+2)}\theta_1'' \cos(\theta_1-\theta_2) - \frac{\eta(\gamma-1)}{(\gamma^2+2)}\theta_1'^2 \sin(\theta_1-\theta_2) + \frac{\eta(\gamma-1)}{(\gamma^2+2)}\Omega_1^2 \sin\theta_2 + d_2\theta_2' = 0 \end{aligned} \quad (21)$$

It should be stressed, that in the previous cases the damping could not be properly controlled due to its nature, whereas in this case, the damping of the tri-pendulum can be properly adjusted to match the optimal performance, especially in the linear case of small vibrations.

The linearized equations of motion are:

$$\begin{aligned} \theta_1'' + \mu\frac{(\gamma-1)}{\eta}\theta_2'' + \Omega_1^2\theta_1 + d_1\theta_1' = -f_1 \\ \theta_2'' + \frac{\eta(\gamma-1)}{(\gamma^2+2)}\theta_1'' + \frac{\eta(\gamma-1)}{(\gamma^2+2)}\Omega_1^2\theta_1 + d_2\theta_2' = 0 \end{aligned} \quad (22)$$

Assuming that $f_1 = F_1 e^{-i\omega t}$ is harmonic and $\theta_1 = X_1 e^{-i\omega t}$ and $\theta_2 = X_2 e^{-i\omega t}$we get the following matrix equations:

$$\begin{bmatrix} \Omega_1^2 - \omega^2 + i\omega d_1 & -\frac{\omega^2\mu(\gamma-1)}{\eta} \\ -\frac{\omega^2\eta(\gamma-1)}{\gamma^2+2} & -\omega^2 + \frac{\eta(\gamma-1)}{\gamma^2+2}\Omega_1^2 + i\omega d_2 \end{bmatrix} \begin{bmatrix} X_1 \\ X_2 \end{bmatrix} = \begin{bmatrix} -F_1 \\ 0 \end{bmatrix} \quad (23)$$

Solving the above linear problem we get the amplitude formulas for the payload and the absorber respectively:

$$A_1 = |X_1| = \left| \frac{-\omega^2 + \frac{\eta(\gamma-1)}{\gamma^2+2}\Omega_1^2 + i\omega d_2}{D} \right| F_1 \quad (24)$$

$$A_2 = |X_2| = \left| \frac{\omega^2\eta(\gamma-1)}{D(\gamma^2+2)} \right| F_1 \quad (25)$$

Where

$$D = (\Omega_1^2 - \omega^2 + i\omega d_1)\left(-\omega^2 + \frac{\eta(\gamma-1)}{\gamma^2+2}\Omega_1^2 + i\omega d_2\right) - \frac{\omega^4\mu(\gamma-1)^2}{\gamma^2+2} \quad (26)$$

It is well-known that tuning of a tuned mass damper follows the work by Den Hartog [34], whereby the frequency ratio of the absorber over the primary system should be equal to $1/(1+\mu)$. Applying this condition to the herein absorber, we arrive at the following condition:

$$\gamma^2 - \eta(1+\mu)^2\gamma + \eta(1+\mu)^2 + 2 = 0 \quad (27)$$

which has two exact solutions for γ. Figure 10 left presents the curves of $\gamma(\eta)$ for three different values of μ and indicates that the desirable low values of γ, which is responsible for the size of the tri-pendulum, can be attained at high values of η, responsible for the ratio between the length of the payload and the size of the tri-pendulum. For example, η=10 indicates that h_2 is one order of magnitude smaller than the payload swinging length, and the corresponding γ around 1.3, which is a broadly realistic scenario. It should be stressed that these values can be achieved almost independently of the mass ratio, which should be as small as possible in this case. Figure 10 right shows a parametric plot of the (η, μ) parameter pair. The shaded region denotes the area where Eq. (27) has real solutions in γ, given by $\eta_{lim} = 2(1+\sqrt{3})/(1+\mu)^2$. Essentially, this limiting value defines the descent length limits for which the proposed absorber can be realistically designed to mitigate the payload vibrations. In the unshaded region, the absorber design cannot be realized. Note that this is the limiting case of a realistic design with, nevertheless, dubious performance. It does, however, indicate that the absorber is effective for the descent lengths that correspond to approximately $\eta > 5.5$ for limiting small absorber mass. This is favourable for the considered application, since the payload sway becomes more prominent at relatively large lengths.

Formatted: Font: 12 pt

Comment [YD4]: Add here how it is related to the absorber size!

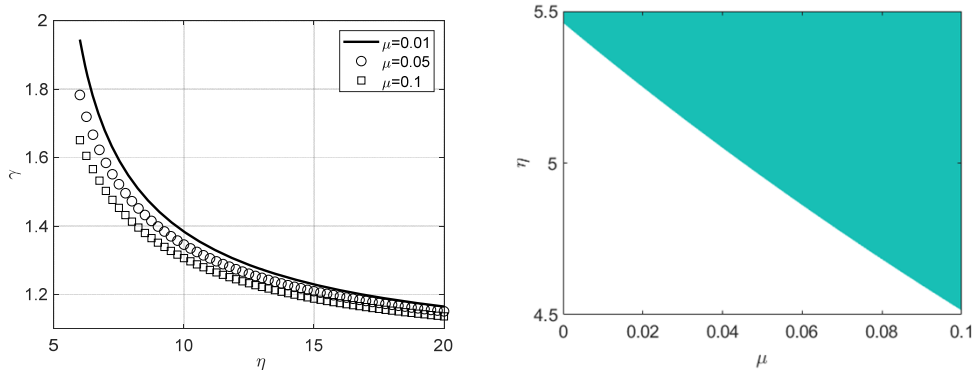

Figure 10. Values of γ vs η (left) and the minimum η values to have the maximum absorber size (right).

The tuning procedure has so far considered the well-known Den Hartog approach. However, this approach is derived for an undamped primary system, which might lead to significant deviation from the desired performance when damping is taken into account. In Figure 11, the optimum γ is found by direct assessment of the payload response amplitude for $\omega = \Omega$. Whereas Den Hartong tuning would recommend γ =1.3456, whereas visual inspection of Figure 11a reveals that the optimal value is γ =1.3944. This is also confirmed by the frequency response of the coupled system for μ =0.05 in Figure 11b, which shows that numerical tuning leads to more than twice more effective reduction of the payload response amplitude.

Formatted: Font: 12 pt

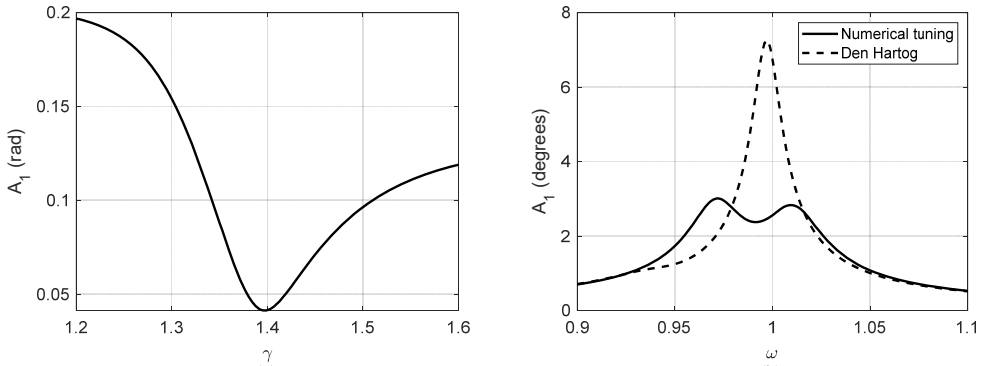

Figure 11. Figures (a) Response amplitude at $\omega = \Omega$ against γ for μ =0.05; (b) Comparison of the frequency response for Den Hartog tuning (dashed) and for numerical tuning (solid).

The next step in the analysis considers the selection of the absorber damping, d_2. Figure 12 shows bivariate surface plots of the payload response amplitude against frequency ω and absorber damping, d_2, for three representative values of η. The surface plots reveal a similar pattern across the examined cases of bi-modal response curve in the lightly damped region and a transition to a unimodal one as damping increases. In fact, the turning point between the two response types carries favourable characteristics for vibration absorption, such as limited peak response and nearly flat response curve across the primary resonance frequency range, between the peak frequency values.

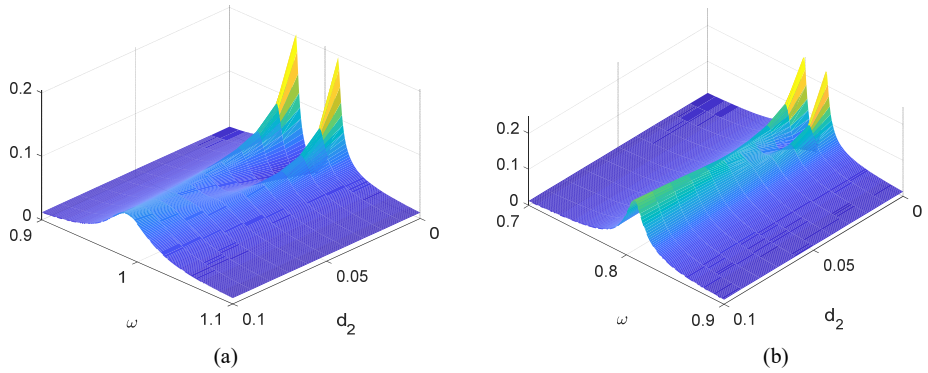

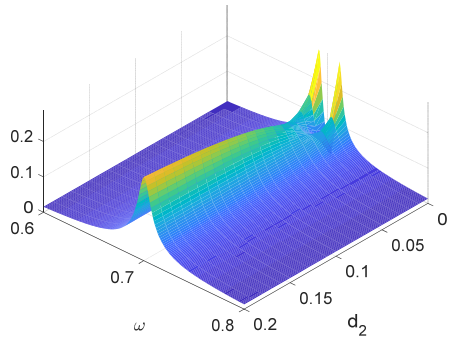

(c)

Figure 12. Surface plots of the response amplitude A_1 versus ω and d_2 for optimal gamma, F_1=0.002, μ=0.05 and d_1=0.05; (a) η=10; (b) η =15; (c) η =20;

Figure 13a reveals the impact of the absorber damping on the structure of the frequency response, showing that damping increases towards a critical value where the curve is nearly flat within the resonant range (for $d_2 = 0.08$). Moreover, the maximum amplitude is around 2 degrees whereas the primary system without the absorber would sway at more than 11 degrees under the same conditions. One can notice though that the optimal damping value is not constant for all η values. It is evident in Figure 12 that as η increases, the critical damping value becomes smaller. This poses the question of the absorber performance during the payload descent, and how the optimal damping value could impact the payload amplitude reduction. Figure 13b shows frequency response curves for $d_2 = 0.04$ and various descent lengths between $\eta = 10$ and $\eta = 20$. Although the performance varies, the response amplitude near the resonant region remains multiple times lower when compared with the primary system response. This plots injects confidence that the proposed pendulum absorber can remain extremely efficient for low-amplitude vibrations, even if it is designed as a purely passive system.

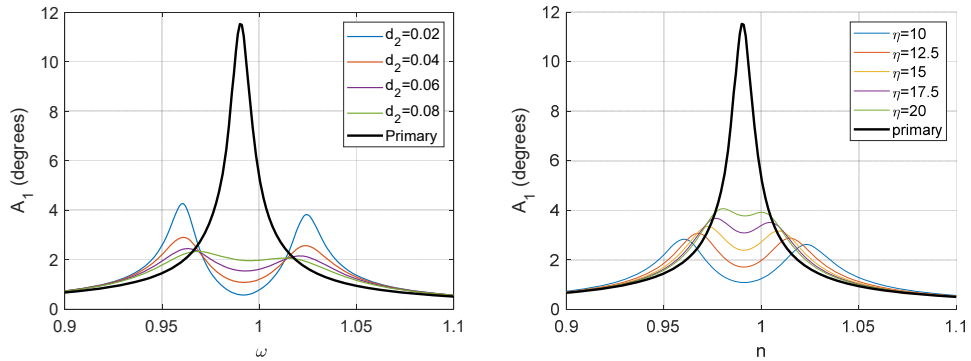

Figure 13. Frequency response curves for F_1=0.002, μ=0.05 and d_1=0.05; (a) $\eta = 10$ and varying d_2;(b) $d_2 = 0.04$ and varying η.

6 Conclusions

In this work pendulum tuned mass damper was proposed to be utilised as a nonlinear energy

absorber for mitigating vibrations of the payload, modelled as a lumped mass pendulum. First, the pendulum absorber was proposed to be placed between the payload and the suspension point. While this concept was a very attractive option, which required no significant changes to the existing crane designs, it proved to be no effective for low mass values of the absorber. Second studied concept, which proposed to place the absorber under the payload, proved to be very effective when the distance between the suspension point and the payload is equal to the distance between the payload and absorber. This concept can significantly mitigate the vibration amplitude of the payload, however it has a limited practical application. The reason is that at the begging of lifting the absorber will not be effective at all resting on the ground or water, until the payload passes the half-distance. Thus, the third design was proposed, which used the concept of tri-pendulum connected to a lifting cage. In this case it becomes possible to tune the tri-pendulum to a required frequency for mitigating the oscillations by changing the parameters of the tri-pendulum and embedded damping. In fact, the tri-pendulum can operate form the very beginning of hoisting and can be online adjusted by moving the tri-pendulum masses along their arms.

References

[1] T. G. Vaughters and M. F. Mardiros. Joint logistics over the shore operations in rough seas. Naval Engineers Journal, 1997, 109(3):385-393.

[2] Witz J.A. Parametric excitation of crane loads in moderate sea states. Ocean Engineering, 22(4):411 - 420, 1995.

[3] Ellermann K., Kreuzer E., and Marian Markiewicz. Nonlinear dynamics of floating cranes. Nonlinear Dynamics, 27(2):107-183, 2002.

[4] M. Idres, K. Youssef, D. Mook, and A. Nayfeh. A nonlinear 8-dof coupled crane-ship dynamic model. In 44th AIAA/ASME/ASCE/AHS/ASC Conference, pages 670-675. ASME, 2003.

[5] E.M. Abdel-Rahman, A.H. Nayfeh, Z.N. Masoud. Dynamics and control of cranes: a review. J. Vib. Control., 9 (2003), pp. 863-908.

[6] A Alfi, A Shokrzadeh, M Asadi. Reliability analysis of H-infinity control for a container ship in way-point tracking. Applied Ocean Research, 2015

[7] Ievgen Golovin, Stefan Palis. Robust control for active damping of elastic gantry crane vibrations. Mechanical Systems and Signal Processing, 121, 2019

[8] G Xia, T Luan. Study of ship heading control using RBF neural network. International Journal of Control and Automation, 2015.

[9] Liyana Ramli, Z. Mohamed, H. I. Jaafar. A neural network-based input shaping for swing suppression of an overhead crane under payload hoisting and mass variations. Mechanical Systems and Signal Processing,107,2018

[10] Ning Sun, Yongchun Fang, He Chen, Yiming Wu, Biao Lu. Nonlinear Antiswing Control of Offshore Cranes With Unknown Parameters and Persistent Ship-Induced Perturbations: Theoretical Design and Hardware Experiments. IEEE Transactions on Industrial Electronics, 65(3), 2017.

[11] Ning Sun, Yiming Wu, Xiao Liang, Yongchun Fang. Nonlinear Stable Transportation

Control for Double-Pendulum Shipboard Cranes with Ship-Motion-Induced Disturbances. IEEE Transactions on Industrial Electronics, 66(12), 2019.

[12] Xianqing Wu, Kexin Xu, Xiongxiong He. Disturbance-observer-based nonlinear control for overhead cranes subject to uncertain disturbances. Mechanical Systems and Signal Processing, 139, 2020

[13] Y Qian, Y Fang, B Lu. Adaptive robust tracking control for an offshore ship-mounted crane subject to unmatched sea wave disturbances. Mechanical Systems and Signal Processing, 2019.

[14] Viet Duc La, Kien Trong Nguyen. Combination of input shaping and radial spring-damper to reduce tridirectional vibration of crane payload. Mechanical Systems and Signal Processing,116, 2019Ning Sun, Yiming Wu, He Chen, Yongchun Fang. An energy-optimal solution for transportation control of cranes with double pendulum dynamics: Design and experiments. Mechanical Systems and Signal Processing,102, 2018.

[15] M.J.Maghsoudi, Liyana Ramli, S.Sudin, Z.Mohamed, A.R.Husain, H.Wahidb. Improved unity magnitude input shaping scheme for sway control of an underactuated 3D overhead crane with hoisting. Mechanical Systems and Signal Processing,123, 2019.

[16] Xinsheng Zhao, Jie Huang. Distributed-mass payload dynamics and control of dual cranes undergoing planar motions. Mechanical Systems and Signal Processing, 126, 2019

[17] Khorshid, Emad, Abdulaziz Al-Fadhli, Khalid Alghanim, and Jasem Baroon. “Command Shaping with Reduced Maneuvering Time for Crane Control.” Journal of Vibration and Control, 2020.

[18] Ning Sun, Yiming Wu, He Chen, Yongchun Fang. An energy-optimal solution for transportation control of cranes with double pendulum dynamics: Design and experiments. Mechanical Systems and Signal Processing,102, 2018.

[19] Qingxiang Wu, Xiaokai Wang, Lin Hua, Minghui Xia. Dynamic analysis and time optimal anti-swing control of double pendulum bridge crane with distributed mass beams. Mechanical Systems and Signal Processing, 144, 2020.

[20] Okubanjo, A, Oyetola, O, Adekomaya, O, Vision based control of gantry crane system. Anadolu University of Sciences & Technology - A: Applied Sciences & Engineering. 19(4), 2018.

[21] Le Anh Tuan, Soon-Geul Lee. Modeling and advanced sliding mode controls of crawler cranes considering wire rope elasticity and complicated operations. Mechanical Systems and Signal Processing, 103, 2018.

[22] Shengzeng Zhang, Xiongxiong He, Haiyue Zhu, Qiang Chen, Yuanjing Feng. Partially saturated coupled-dissipation control for underactuated overhead cranes. Mechanical Systems and Signal Processing, 136, 2020.

[23] Aboserre, Lobna T., and Ayman A. El-Badawy. “Robust Integral Sliding Mode Control of Tower Cranes.” Journal of Vibration and Control, 2020.

[24] Shengzeng Zhang, Xiongxiong He, Qiang Chen, Zhengyang Zhu, Partially saturated coupling-based control for underactuated overhead cranes with experimental verification,

Mechatronics, Volume 63, 2019.

[25] Menghua Zhang, Yongfeng Zhang, He Chen, Xingong Cheng. Model-independent PD-SMC method with payload swing suppression for 3D overhead crane systems. Mechanical Systems and Signal Processing, 129, 2019

[26] Roger Miranda-Colorado, Luis T. Aguilar. A family of anti-swing motion controllers for 2D-cranes with load hoisting/lowering. Mechanical Systems and Signal Processing, 133, 2019.

[27] D Yurchenko, P Alevras. Stability, control and reliability of a ship crane payload motion. Probabilistic Engineering Mechanics 38, 173-179, 2014.

[28] Liyana Ramli, Z. Mohamed, M. Ö. Efe, Izzuddin M. Lazim, H. I. Jaafar. Efficient swing control of an overhead crane with simultaneous payload hoisting and external disturbances. Mechanical Systems and Signal Processing, 135, 2020

[29] A.M.Abdullahi, Z.Mohamed, H.Selamat, H.R.Pota, M.S.Zainal Abidin, S.M.Fasih. Efficient control of a 3D overhead crane with simultaneous payload hoisting and wind disturbance: design, simulation and experiment, 145, 2020.

[30] P. Hyla. The crane control systems: a survey. 17th Int. Conf. Methods Model. Autom. Robot., Miedzyzdroje, Poland (2012), pp. 505-509

[31] Liyana Ramli, Z. Mohamed, Auwalu M. Abdullahi, H.I. Jaafar, Izzuddin M. Lazim. Control strategies for crane systems: A comprehensive review, 95, 2017.

[32] R.L. Mohamed, Z. Abdullahi, A.M. Jaafar, H.I. Lazim, I.M., Control strategies for crane systems: A comprehensive review, Mechanical Systems and Signal Processing, Vol. 95, pp. 1-23, 2017.

[33] Keum-Shik Hong, Umer Hameed Shah. Dynamics and Control of Industrial Cranes. 2019.

[34] Den Hartog JP (2013) Mechanical vibrations. Courier Dover Publications, New York

[35] D Yurchenko. Tuned Mass and Parametric Pendulum Dampers Under Seismic Vibrations. Encyclopedia of Earthquake Engineering. 2015.

[36] Rafael H. Lopez, Leandro F. F. Miguel, André T. Beck. Tuned Mass Dampers for Passive Control of Structures Under Earthquake Excitations. Encyclopedia of Earthquake Engineering. 2015.

[37] R.A.Ibrahim. Recent advances in nonlinear passive vibration isolators. Journal of Sound and Vibration. Volume 314, Issues 3–5, 22 July 2008, pp. 371-452.

[38] A.F. Vakakis, O.V. Gendelman, L.A. Bergman, D.M. McFarland, G. Kerschen, Y.S. Lee. Nonlinear Targeted Energy Transfer in Mechanical and Structural Systems. Springer, 2008.

[39] Troy Shinbrot, Celso Grebogi, Jack Wisdom, James Yorke. Chaos in a double pendulum. American Journal of Physics, American Association of Physics Teachers, 1992, 60, pp.491 - 491

[40] R. B. Levien, S.M Tan. Double pendulum: An experiment in chaos. January 1993. American Journal of Physics 61(11):1038-1044

[41] A.V. Ivanov. Study of the double mathematical pendulum - i: numerical investigation of homoclinic transversal intersections. Regular and Chaotic Dynamics, 4(1), 1999.

[42] AV Ivanov Study of the Double Mathematical Pendulum II Investigation of Exponentially Small Homoclinic Intersections. Journal of physics A: mathematical and general, 34, 2001.

[43] T. Stachowiak, W. Szuminski. Non-integrability of restricted double pendula. Physics Letters A 379 (2015) 3017–3024.

[44] H.R. Dullin. Melnikov's method applied to the double pendulum. Zeitschrift für Physik B Condensed Matter, 93, pp. 521–528, 1994.

[45] AV Ivanov. Study of the Double Mathematical Pendulum-III: Menikov's Method Applied to the System in the Limit of Small Ratio of Pendulums Masses. Regular and Chaotic Dynamics, 5(3), 2000.

[46] R. Kwiatkowski. Movement of double mathematical pendulum with variable mass, Machine Dynamics Research, 38 2 (2014) 47-58.

[47] R. Kwiatkowski. Dynamic analysis of double pendulum with variable mass and initial velocities. Procedia Engineering, 136, (2016), 175 – 180.

[48] R. Kwiatkowski. Dynamics of a double mathematical pendulum with variable mass in dimensionless coordinates. Procedia Engineering, 177, (2017), 439 – 443.

[49] JC Sartorelli, W Lacarbonara. Parametric resonances in a base-excited double pendulum. Nonlinear Dynamics, 69(4), 2012.

[50] Rahul Kumar, Sayan Gupta, Shaikh Faruque Ali. Energy harvesting from chaos in base excited double pendulum, Mechanical Systems and Signal Processing, 124, 2019.

[51] D Yurchenko, P Alevras. Dynamics of the N-pendulum and its application to a wave energy converter concept. International Journal of Dynamics and Control, 1(4), 290-299, 2013

APPENDIX

In this appendix the governing equations of motion will be derived for the undamped systems for all three cases considered in the paper.

The equation of motion for the Case I and Case II.

To derive the equation of motion of a pendulum with a moving suspension point in vertical (w) and horizontal (z) direction one can use the Lagrange approach:

$$\frac{d}{dt}\left(\frac{\partial L}{\partial \dot{q}_i}\right) - \frac{\partial L}{\partial q_i} = 0,\ L = T - U \tag{A1}$$

with $i = 1,2,\ q_i = \theta_i$.

From geometry one can write:

$$x_1 = L_1 \sin\theta_1,\ \ y_1 = L_1 \cos\theta_1 \tag{A2}$$

$$x_2 = L_1 \sin\theta_1 + L_2 \sin\theta_2,\ \ y_2 = L_1 \cos\theta_1 + L_2 \cos\theta_2 \tag{A3}$$

The potential and kinetic energies are:

$$\begin{aligned} U &= -(m+M) g L_1 \cos\theta_1 - M g L_2 \cos\theta_2, \\ T &= \frac{m}{2}(\dot{x}_1^2 + \dot{y}_1^2) + \frac{M}{2}(\dot{x}_2^2 + \dot{y}_2^2) \end{aligned} \tag{A4}$$

$$T = \frac{m+M}{2}\left(L_1\dot{\theta}_1\right)^2 + \frac{M}{2}\left(L_2\dot{\theta}_2\right)^2 + M L_1 L_2 \dot{\theta}_1 \dot{\theta}_2 \cos(\theta_2 - \theta_1) \tag{A5}$$

Then,

$$\frac{\partial T}{\partial \dot{\theta}_1} = (m+M) L_1^2 \dot{\theta}_1 + M L_1 L_2 \dot{\theta}_2 \cos(\theta_2 - \theta_1) \tag{A6}$$

$$\frac{d}{dt}\left(\frac{\partial T}{\partial \dot{\theta}_1}\right) = (m+M) L_1^2 \ddot{\theta}_1 + M L_1 L_2 \ddot{\theta}_2 \cos(\theta_2 - \theta_1) - M L_1 L_2 \dot{\theta}_2 \sin(\theta_2 - \theta_1)(\dot{\theta}_2 - \dot{\theta}_1) \tag{A7}$$

$$\frac{\partial T}{\partial \dot{\theta}_2} = M L_2^2 \dot{\theta}_2 + M L_1 L_2 \dot{\theta}_1 \cos(\theta_2 - \theta_1) \tag{A8}$$

$$\frac{d}{dt}\left(\frac{\partial T}{\partial \dot{\theta}_2}\right) = M\left(L_2^2 \ddot{\theta}_2 + L_1 L_2 \ddot{\theta}_1 \cos(\theta_2 - \theta_1) - L_1 L_2 \dot{\theta}_1 \sin(\theta_2 - \theta_1)(\dot{\theta}_2 - \dot{\theta}_1)\right) \tag{A9}$$

$$\frac{\partial T}{\partial \theta_1} = M L_2 L_1 \dot{\theta}_1 \dot{\theta}_2 \sin(\theta_2 - \theta_1) \tag{A10}$$

$$\frac{\partial T}{\partial \theta_2} = -M L_1 \dot{\theta}_1 L_2 \dot{\theta}_2 \sin(\theta_2 - \theta_1) \tag{A11}$$

$$\frac{d}{dt}\left(\frac{\partial U}{\partial \dot{\theta}_1}\right) = 0,\ \ \frac{\partial U}{\partial \theta_1} = (m+M) g L_1 \sin\theta_1,\ \ \frac{\partial U}{\partial \theta_2} = M g L_2 \sin\theta_2 \tag{A12}$$

In the case of a free undamped response the governing equations of motion are:

$$\begin{aligned} \frac{d}{dt}\left(\frac{\partial L}{\partial \dot{q}_1}\right) - \frac{\partial L}{\partial q_1} &= (m+M) L_1^2 \ddot{\theta}_1 + M L_1 L_2 \ddot{\theta}_2 \cos(\theta_2 - \theta_1) - \\ -M L_1 L_2 \dot{\theta}_2^2 \sin(\theta_2 - \theta_1) &+ (m+M) g L_1 \sin\theta_1 = 0 \end{aligned} \tag{A13}$$

$$\frac{d}{dt}\left(\frac{\partial L}{\partial \dot{q}_2}\right) - \frac{\partial L}{\partial q_2} = ML_2^2\ddot{\theta}_2 + ML_1L_2\ddot{\theta}_1\cos(\theta_2 - \theta_1) + \\ +ML_1L_2\dot{\theta}_1^2\sin(\theta_2 - \theta_1) + MgL_2\sin\theta_2 = 0 \quad \text{(A14)}$$

When an external force is applied to each mass the equations, they can be added to the corresponding equations. Introducing the nondimensional mass $\mu = \frac{M}{M+m}$ and length $\eta = \frac{L_1}{L_2}$ ratios and diving equation (A13) by $(m+M)L_2$ and equation (A14) by ML_2^2 one arrives to the following set of equations ($\Omega_2^2 = g/L_2$):

$$\eta\ddot{\theta}_1 + \mu\ddot{\theta}_2\cos(\theta_2 - \theta_1) - \mu\dot{\theta}_2^2\sin(\theta_2 - \theta_1) + \Omega_2^2\sin\theta_1 = -\mu\frac{F_2}{M_2L_2}cos(\theta_2 - \theta_1) - \frac{\mu}{L_2}\frac{F_1}{M_2} \quad \text{(A15)}$$

$$\ddot{\theta}_2 + \eta\cos(\theta_2 - \theta_1)\cdot\ddot{\theta}_1 + \eta\dot{\theta}_1^2 sin(\theta_2 - \theta_1) + \Omega_2^2 sin\theta_2 = -\frac{F_2}{M_2L_2} \quad \text{(A16)}$$

which agree with the set of equation (8) developed by Newton's approach. To decouple the equations coupled by accelerations, let's move all the terms except the acceleration to the right side of equations:

$$\eta\ddot{\theta}_1 + \mu\ddot{\theta}_2\cos(\theta_2 - \theta_1) = F \quad \text{(A17)}$$

$$\eta\ddot{\theta}_1\cos(\theta_2 - \theta_1) + \ddot{\theta}_2 = G \quad \text{(A18)}$$

where:

$$F = \mu\dot{\theta}_2^2\sin(\theta_2 - \theta_1) - \Omega_2^2\sin\theta_1 - \mu\frac{F_2}{M_2L_2}cos(\theta_2 - \theta_1) - \frac{\mu}{L_2}\frac{F_1}{M_2} \quad \text{(A19)}$$

$$G = -\eta\sin(\theta_2 - \theta_1)\dot{\theta}_1^2 - \Omega_2^2\sin\theta_2 - \frac{F_2}{M_2L_2} \quad \text{(A20)}$$

Introducing the variable $J = \eta[1 - \mu\cos^2(\theta_1 - \theta_2)]$ one can rewrite the equation (A17) and (A18) as:

$$\ddot{\theta}_1 = \frac{F - G\mu\cos(\theta_1 - \theta_2)}{J\eta} \quad \text{(A21)}$$

$$\ddot{\theta}_2 = \frac{G - F\cos(\theta_1 - \theta_2)}{J} \quad \text{(A22)}$$

The equation of motion for Case III.

From the geometrical considerations one can express the tri-pendulum dynamic as following:

$$x_1 = L_1\sin\theta_1, \;\; y_1 = L_1\cos\theta_1 \quad \text{(A23)}$$

$$\begin{cases} z_1 = L_1\sin\theta_1 + h_1\sin\theta_2, \;\; w_1 = L_1\cos\theta_1 + h_1\cos\theta_2 \\ z_2 = L_1\sin\theta_1 + h_2\cos(\theta_2 + 30), \;\; w_2 = L_1\cos\theta_1 - h_2\sin(\theta_2 + 30) \\ z_3 = L_1\sin\theta_1 - h_3\sin(\theta_3 - 30), \;\; w_3 = L_1\cos\theta_1 + h_3\sin(\theta_3 - 30) \end{cases} \quad \text{(A24)}$$

Differentiating with respect to time each of the above variable to obtain the corresponding velocities one can get the following expressions for kinetic and potential energy, assuming that $M_1 = M_2 = M_3 = M$:

$$T = \frac{m}{2}(\dot{x}_1^2 + \dot{y}_1^2) + \frac{M}{2}(\dot{z}_1^2 + \dot{w}_1^2) + \frac{M}{2}(\dot{z}_1^2 + \dot{w}_1^2) + \frac{M}{2}(\dot{z}_1^2 + \dot{w}_1^2) = \\ = \frac{m+3M}{2}L_1^2\dot{\theta}_1^2 + \frac{M}{2}[h_1^2 + h_2^2 + h_3^2]\dot{\theta}_2^2 + \\ +ML_1\dot{\theta}_1\,\dot{\theta}_2\,[h_1\cos(\theta_1 - \theta_2) + h_2\sin(\theta_1 - \theta_2 - 30) - h_3\sin(\theta_1 - \theta_2 + 30)] \quad \text{(A25)}$$

For h_2=h_3 and using the trigonometric properties the above expression can be reduced to the following expression.

$$T = \frac{m+3M}{2} L_1^2 \dot{\theta}_1^2 + \frac{M}{2}[h_1^2 + 2h_2^2]\dot{\theta}_2^2 - ML_1\dot{\theta}_1\ \dot{\theta}_2\ [h_1 - h_2]\cos(\theta_1 - \theta_2) \quad \text{(A26)}$$

The potential energy of the system is:

$$\begin{gathered} U = (m+3M)gL_1(1-\cos\theta_1) + Mg[h_1(1-\cos\theta_2) + \\ +h_2(\sin(30+\theta_2) - \sin 30) - h_3(\sin(30) - \sin(30-\theta_2))] = \\ = (m+3M)gL_1(1-\cos\theta_1) + Mg(1-\cos\theta_2)[h_1 - h_2] \end{gathered} \quad \text{(A26)}$$

Then, the

$$\frac{\partial T}{\partial \dot{\theta}_1} = (m+3M)L_1^2\dot{\theta}_1 + ML_1[h_1 - h_2]\dot{\theta}_2\cos(\theta_2 - \theta_1) \quad \text{(A27)}$$

$$\begin{gathered} \frac{d}{dt}\left(\frac{\partial T}{\partial \dot{\theta}_1}\right) = (m+3M)L_1^2\ddot{\theta}_1 + ML_1[h_1 - h_2]\ddot{\theta}_2\cos(\theta_2 - \theta_1) - \\ -ML_1[h_1 - h_2]\dot{\theta}_2\sin(\theta_2 - \theta_1)(\dot{\theta}_2 - \dot{\theta}_1) \end{gathered} \quad \text{(A28)}$$

$$\frac{\partial T}{\partial \dot{\theta}_2} = M[h_1^2 + 2h_2^2]\dot{\theta}_2 + ML_1[h_1 - h_2]\dot{\theta}_1\cos(\theta_2 - \theta_1) \quad \text{(A29)}$$

$$\begin{gathered} \frac{d}{dt}\left(\frac{\partial T}{\partial \dot{\theta}_2}\right) = M\Big[[h_1^2 + 2h_2^2]\ddot{\theta}_2 + L_1[h_1 - h_2]\ddot{\theta}_1\cos(\theta_2 - \theta_1\Big) - \\ -L_1[h_1 - h_2]\dot{\theta}_1\sin(\theta_2 - \theta_1)(\dot{\theta}_2 - \dot{\theta}_1)] \end{gathered} \quad \text{(A30)}$$

$$\frac{\partial T}{\partial \theta_1} = M[h_1 - h_2]L_1\dot{\theta}_1\dot{\theta}_2\sin(\theta_2 - \theta_1) \quad \text{(A31)}$$

$$\frac{\partial T}{\partial \theta_2} = -ML_1\dot{\theta}_1[h_1 - h_2]\dot{\theta}_2\sin(\theta_2 - \theta_1) \quad \text{(A32)}$$

$$\frac{\partial U}{\partial \theta_1} = (m+3M)gL_1\sin\theta_1,\ \ \frac{\partial U}{\partial \theta_2} = Mg[h_1 - h_2]\sin\theta_2 \quad \text{(A33)}$$

In the case of a free undamped response the governing equations of motion are:

$$\begin{gathered} \frac{d}{dt}\left(\frac{\partial L}{\partial \dot{q}_1}\right) - \frac{\partial L}{\partial q_1} = (m+3M)L_1^2\ddot{\theta}_1 + ML_1[h_1 - h_2]\ddot{\theta}_2\cos(\theta_2 - \theta_1) + \\ +ML_1[h_1 - h_2]\dot{\theta}_2^2\sin(\theta_2 - \theta_1) + (m+3M)gL_1\sin\theta_1 = 0 \end{gathered} \quad \text{(A34)}$$

$$\begin{gathered} \frac{d}{dt}\left(\frac{\partial L}{\partial \dot{q}_2}\right) - \frac{\partial L}{\partial q_2} = M[h_1^2 + 2h_2^2]\ddot{\theta}_2 + ML_1[h_1 - h_2]\ddot{\theta}_1\cos(\theta_2 - \theta_1) + \\ +ML_1[h_1 - h_2]\dot{\theta}_1^2\sin(\theta_2 - \theta_1) + Mg[h_1 - h_2]\sin\theta_2 = 0 \end{gathered} \quad \text{(A35)}$$